Publisher: GSA
Journal: GEOL: Geology
Article ID: G34371

Coastline retreat via progressive failure of rocky coastal cliffs

Nick J. Rosser[1], Matthew J. Brain[1], David N. Petley[1], Michael Lim[2], and Emma C. Norman[1]

[1]*Department of Geography, Durham University, South Road, Durham DH1 3LE, UK*

[2]*Engineering and Environment, Northumbria University, Newcastle upon Tyne NE1 8ST, UK*

ABSTRACT

Despite much research on the myriad processes that erode rocky coastal cliffs, accurately predicting the nature, location and timing of coastline retreat remains challenging, confounded by the apparently episodic nature of cliff failure. The dominant drivers of coastal erosion, marine and sub-aerial forcing, are anticipated in future to increase, so understanding their present and combined efficacy is fundamental to improving predictions of coastline retreat. We capture change using repeat laser scanning across 2.7 x 10^4 m^2 of near-vertical rock cliffs on the UK North Sea coast over 7 years to determine the controls on the rates, patterns and mechanisms of erosion. For the first time we document that progressive upward propagation of failure dictates the mode and defines the rate at which marine erosion of the toe can accrue retreat of coastline above; notably a failure mechanism not conventionally considered in cliff stability models. Propagation of instability and failure operates at these sites at 10^1 year timescales and is moderated by local rock mass strength and the time-dependence of rock fracture. We suggest that once initiated, failure propagation can operate ostensibly independently to external environmental forcing, and so may not be tightly coupled to prevailing subaerial and oceanographic conditions. Our observations apply to coasts of both uniform and complex lithology, where failure geometry is defined by rock mass strength and structure, and not intact rock strength alone, and where retreat occurs via any mode other than full cliff collapse.

INTRODUCTION

Global sea-level rise and pole-ward shifts in extra-tropical storm tracks will drive changes to winds, tides, precipitation, storms and wave climate (Nicholls and Cazenave, 2010; Trenhaile, 2011). In this context, coastline retreat will continue to pose a pervasive hazard, not least because of the stochastic nature of failure and step-back of the cliff (Young and Ashford, 2008). This presents a need to understand the mechanisms which define how marine and subaerial forcing drives coastal cliff erosion.

Controls on erosion mechanism and retreat mode are locally specific (Naylor and Stephenson, 2010), resulting from the interaction of rock strength (Sunamura, 1982; Collins and Sitar, 2008; 2011; Dornbusch et al., 2008), structure (Allison and Kimber, 1998), the presence or absence of beach sediments (Limber and Murray, 2011), and the effectiveness of environmental forcing (Adams et al., 2002). On cliffed rocky coasts episodic step-back contrasts with quasi-continuous mass wasting from the face and incremental abrasion of the inundated toe (Emery and Kuhn, 1982).

The geometry and mechanism of step-back by marine undercutting of the toe and cantilever failure is well-understood (e.g., Kogure and Matsukura, 2010), where rock mass strength and/or structure prohibits deep-seated failure. However, the nature of the connection between toe erosion and retreat lacks consensus (Moses and Robinson, 2011), and may vary in time and space. Direct observations of toe attrition and abrasion remain surprisingly sparse (Furlani et al., 2010), and so erosion is often inferred solely from the retreat of the coastline without consideration of mechanisms operating upon the cliff face itself (Ashton et al., 2011). Direct observations of cliff erosion provide tentative insight but also highlight the complexity: failure often occurs without an obvious trigger; notches feature but are far from ubiquitous

questioning the dominance of toe cut driven retreat; spalling is effectively continuous; cliff rockfall volume frequency is power-law distributed and lithology specific (Barlow et al., 2011); and, the role of lithological heterogeneity remains difficult to define (Benumof et al., 2000).

While there are few things more predictable than the rise and fall of the tide, it commonly remains challenging to correlate the rates of cliff erosion to environmental drivers (Hapke and Green, 2006). Although small-scale rockfalls (< 0.1 m^3) show some dependence upon environmental controls (e.g. Rosser et al., 2007) and in focused case studies retreat can be successfully related to local combinations of forcing (e.g. Collins and Sitar, 2008), the timing and triggers of the largest failures remains difficult to identify.

Despite this, evidence for temporal patterns, notably sequenced precursors to rock slope failure, have been identified elsewhere, including spalling (Rosser et al., 2007), creep displacements (Abellán et al., 2009), absence of triggers (Sanderson et al., 1996), and microseismicity (Senfaute et al., 2009), implying an underlying time-dependent process. Intensive numerical modeling of individual rock slopes has demonstrated the evolution of failures resulting from kinematics (Allison and Kimber, 1998) and strength degradation, structural control and undercutting (Styles et al., 2011), yet such processes remain absent from larger scale, abstracted coastal cliff retreat models (e.g. Ashton et al., 2011). How marine and subaerial erosion processes interact, and their relative efficacy in defining the timing of short- and long-term retreat over various spatial scales remains poorly understood (Young et al., 2011). Determining this response depends upon correctly identifying current dominant modes of cliff failure, the mechanism in which erosion processes accrue retreat and explaining observed rockfall patterns, which we seek to ascertain here using periodic high-resolution monitoring over a 7 year period.

STUDY AREA

The cliffs of the North York Moors National Park, UK, (GSA Data repository A & B) are comprised of near-vertical rock faces cut in complex near-horizontally interbedded Lower Jurassic shales and limestones (compressive strength σ_{ucs} = 16.69 MPa), siltstones (σ_{ucs} = 30.20 MPa), mudstones (σ_{ucs} = 41.54 MPa), capped with massively jointed fine-grained sandstone (σ_{ucs} = 34.21 MPa) (Rawson and Wright, 2000). The cliff faces are up to 60 m high, with weathered surfaces, dilated joints and face-parallel fractures. Failed material disintegrates on impact with the foreshore to sub-meter fragments that are rapidly reworked and removed (Lim et al., 2010), leaving negligible beach deposits. The cliffs are fronted by a gently sloping (< 2°) extensibly sediment free foreshore platforms that extends c. 300 m seaward at low tides. No notable foreshore erosion was recorded during this study. The coast is storm dominated and macrotidal, with semi-diurnal tides up to 6 m in range, which with wave set-up inundates up to 4.3 m of the cliff during spring tide storms. Analysis of historic maps published since 1856 shows retreat of 0.05 m yr^{-1} with no indication of profile-form adjustment (Agar, 1960); notably a rate below cartographic precision.

DATA CAPTURE

We used a terrestrial laser scanning positioned with dGPS during low tides annually between 1 September 2003 and 3 September 2010. Seven sites totalling 27,069 m^2 cliff face / 710 m of coastline were scanned at a mean point spacing of between 0.03 and 0.05 m from a range equal to the cliff height, and sequentially registered with RMSE of +/– 0.01 m. Subtraction of sequential scans derives erosion depth normal to the cliff face (*d*) (Rosser et al., 2005). We considered annual and cumulative change only when greater than the combined survey error between scans (Schuerch et al., 2012), here 0.05 m, enabling capture of eroded volumes ≥ 1.0 ×

10^{-4} m^3. Highest astronomical tide (HAT), as the highest inundated elevation, was obtained from gauge observations with wave set-up and transformation modeled (based upon Battjes and Stive, 1985) from offshore (18 km, NNE) wave buoy data, to delimit the wet cliff toe (C_t) from the dry cliff face (C_d) (see: Norman, 2012).

GENERAL OBSERVATIONS

Annual cumulative patterns of rockfall (Fig. 1) show the nature of incremental failure across the cliff face obtained from sequential laser scans. Erosion rates in the inundated toe broadly outpace those of the cliff above, but specific lithologies generate either or both more frequent, larger failures (Fig. 1). Over the monitoring period all sites, excluding D, showed widely distributed scars with no obvious preferential elevation of erosion (Fig. 1, Fig. 2, and GSA Data repository C & D). Small-scale rockfall (< 0.1 m^3) were more frequent than larger failures. Scar morphology indicates both fracturing of rock bridges and discontinuity controlled failure. Although neither the initial nor final survey cliff profiles exhibit clear concave toe notches (excluding F), the toe actively eroded at all sites. Uniquely, Site D experienced a catastrophic failure of the whole cliff face, resulting in an instantaneous step-back of the coastline of up to 13.0 m, releasing > 2,400 m^3 of rock (January 2005). Site D is excluded from the following analysis, but is considered below. By area, 29.6 % of the monitored cliff experienced change to September 2010, and by length, only 4.8% of monitored coastline retreated > 0.05 m. The mean retreat rate across sites was 0.027 m yr^{-1} (standard deviation = 0.029 m yr^{-1}). Rock yield, although variable between sites, averaged 1 m^3 per linear meter of coastline per year, totalling 5.01×10^3 m^3 during the monitored period, despite the low coastline retreat measured.

SPATIAL EVOLUTION OF FAILURES

Our analysis reveals that failure scars evolve through time, with a dominant upward (vertical and sub-vertical) and lateral (within lithology) tendency to their expansion (Fig. 1). Many failure scars grow via failure of their periphery between each survey. Contiguous failure scars coalesce and proximal scars bridge, destabilizing larger areas of rock face above. At some elevations, failure propagation appears inhibited, notably at points coincident with exposure of more massively jointed fine-grained sandstones, mirroring previously observed structural control on rockfall magnitude frequency scaling (Barlow et al., 2011). Crucially, while between any survey period failures appear randomly distributed, there is clear spatial clustering indicative of propagation when rockfall are considered as cumulative through time.

Retreat did not correlate with measures of site geometry (cliff aspect, height or foreshore geometry), but did reflect the exposed area of each rock type. The highest rates of erosion were observed in mudstone (54.8% of cliff area: 23.8% of which eroded to depths > 0.05 m), followed by siltstone (30.1%: 14.1%), shale (10.7%: 15.4%), and sandstone (4.4%: 1.8%). C_t represents 8.4% of the total cliff area, yet released 16.8% of the eroded volume. We note the relative similarity in erosion rate between C_t and C_d. If time-averaged erosion rates continue as observed at these sites, these cliffs would resurface (failure across the entire face) after 28.1 years, retreating the coastline by 0.55 m (GSA Data repository E).

Erosion profiles show net cliff change resulting from the cumulative imprint of rockfall (Fig. 2; GSA Data repository F). Each shows isolated zones of rockfall to a consistent depth defined by face parallel joints. At each site, examples of rockfall activity are recorded ostensibly uncoupled from erosion at the toe. Concave features within the erosion profiles at the limit of inundation were captured at sites A and C – E; no corresponding concave inflection in the cliff morphology profile was observed at these elevations (Fig. 2), implying a disconnect in the

timescale of our monitoring and the cliff morphology. Comparison of morphology and erosion profiles suggests coincidence between profile convexity (overhangs and outcrops) and increased erosion below (Fig. 2). The shape of the erosion profile is multi-scalar, characterized by a gradual reduction in d with elevation over a distance > d above local maxima of d (d_{max}), and below a reduction in d over a distance < d. This pattern of erosion depth fits with the failure of convex features as a function of localized stress concentration (e.g. Stock et al., 2012), removing support from material above. Sites B, C and G experienced cliff toe erosion that was continuous in depth up-profile to 24.2 m, 25.9 m, and 21.8 m, respectively. Sites with buttressed toes (A - C) eroded extensively (locally d ≈3 – 5 m), implying cliff steepening as the buttress eroded; near-vertical profiles show more distributed erosion across the face (E - G), implying cliff-parallel retreat.

DISCUSSION

Our data show that the dominant mode of failure on these cliffs is shallow depth rockfall which, after initial triggering by predominantly marine erosion and secondarily by sub-aerial mass wasting, propagate up-cliff where kinematically permissible in a manner moderated by local lithological strength, rock mass architecture and subaerial processes. Coastline retreat results only when either failure on the face extends to the crest, which may require sequential failures to coalesce or superimpose, to exceed local structural control, or when the full face collapses due to undercutting (site D). If the rates of vertical propagation continue as observed, full failure propagation from toe to crest occurs here over a period of 10^1 - 10^2 yrs, notably a period comparable to or longer than most high-resolution monitoring.

Insight into the rates and pattern of failure propagation on rock slopes has been gained by recent studies of progressive collapse inland. Examining pre-failure strain, Abellán et al., (2009)

captured 45 mm of creep over 8 months prior to a 50 m^3 rockfall, and more recently Stock et al., (2012) observed a rockfall sequence in Yosemite over a 1.2 year period, attributing failure evolution to progressive fracture and feedbacks with subaerial processes. Numerically, Styles et al., (2011) modeled time-dependent strain development and strength degradation to analyze rock mass response to 'notching' generating progressive tensile failure and plastic strains. Wolters and Müller (2008) suggest that high cliff toe shear stresses reduce by 75% within 5 m from the toe along the slip path, generating strain as incipient fractures which must be accommodated elsewhere in the rock mass. Sustaining a steep cliff toe via small failures will act to reinforce high re-entrant corner stresses, a control on stability suggested to be as influential as notching itself. Our data suggests that progressive incremental failure is manifest as rockfall in: a zone proximal to the cliff toe; around convexities; and, proximal to previous failures, a mechanism similar to stress relief controlled failures in weaker sands (Hampton, 2002). Implicitly, an eroding toe need not achieve concavity to initiate failure given favorable rock mass structure; hence the lack of toe notching may not preclude a predominance of marine erosion in either defining cliff form or coastline retreat above.

While the precise patterns of events we report here are specific to our sites, we argue that the underlying mechanism has far wider reaching application. Where sub-aerial processes are aggressive, marine driven erosion may only ever be subsumed or outpaced by spalling, generating quasi-continuous retreat. Removing mass, incremental wasting further reduces the likelihood of broader cantilever collapse. Conversely, weathering may act as a catalyst, promoting the upward transmission of erosion via preparation of the cliff face above. Failure can enable direct connectivity from toe to crest, as seen in full collapse of weakly lithified sandstone (Collins and Sitar, 2008) or in chalk cliffs (Senfaute et al., 2009). Where large-scale failure was

observed here (site D), a densely jointed weak mudstone layer is coincident with HAT, promoting locally high toe incision, providing favorable concave geometry to drive deeper-seated / cantilever failure. Small-scale toe failure either triggers an instantaneous larger cascade from above, destabilizing a volume of weathered material (Allison and Kimber, 1998), or stalls where restricted by stable structure; a divergence that must confute relationships between short-term marine forcing and resultant retreat. Such nonlinear feedbacks in rock slopes make predictions or generalizations challenging (Viles, 2013).

Critically, the majority of cliff stability models do not consider progressive fracture and failure, and rarely retain the resolution to allow shallow rockfalls to evolve, to exploit inherent structure, and then propagate upslope. As a result, over the short-term present notch driven cliff failure models define an episodic process of retreat primarily as they are mechanically incapable of simulating the dominant progressive processes we observe. This interpretation can be entirely but incorrectly supported by analysis of monitoring data collated over a single epoch, which does not elucidate failure evolution. As sub-aerial processes, abrasion and fracture dynamics each exploit different facets of rock mass strength, a direct link between intact rock strength, environment, failure mode and rate of retreat will remain difficult to isolate.

Although anecdotal evidence of progressive failure on coastal cliffs is commonplace, few studies on coasts or elsewhere define the rates over which this process operates (e.g. Oppikofer et al., (2008)). Our observations imply over the short-term, a period over which management decisions apply ($10^{\circ} – 10^{2}$ yr), that the timing of cliff failure may more closely reflect progressive rock mass deformation, rather than environment forcing, in line with previous attempts to correlate erosion to environmental drivers (e.g. Lim et al., 2010). The rate, controls

and variability of rock mass deformation remain poorly understood yet can clearly vary between an immediately triggered response, to a process that evolves over decades or more.

Present models of cliff retreat may derive equivalent long-term retreat to that observed here, despite replying on simplified retreat mechanisms, but for rock cliffs such models do not capture the timing and scale of episodic events which may act to protract risks attributed to step-back. As assessing the probability and nature of episodic step-back is arguably as valuable as defining mean retreat, future efforts to model erosion where this mode of failure is active should explore this mechanism. A challenge for future developments to multi-decadal scale cliff retreat models might include algorithms capable of forecasting episodic step-back, while continuing their core-function of abstracting broader representations of coastal evolution. More widely, our observations may hold true for the evolution of non-coastal slopes where undercutting and mass wasting compete, including waterfalls, paraglacial slopes, gorges or river banks.

ACKNOWLEDGMENTS

We thank Cleveland Potash Ltd. for continued support of this research. dGPS network solutions were provided via NERC GEF. Access to wave buoy (PD Ports Ltd, Teesside) and tide-gauge (www.pol.ac.uk) data is gratefully appreciated.

REFERENCES CITED

Abellán, A., Jaboyedoff, M., Oppikofer, T., and Vilaplana, J.M., 2009, Detection of millimetric deformation using a terrestrial laser scanner: Experiment and application to a rockfall event: Natural Hazards and Earth Surface Science, v. 9, p. 365–372, doi:10.5194/nhess-9-365-2009.

228 Adams, P.N., Anderson, R.S., and Revenaugh, J., 2002, Microseismic measurement of wave
229 energy delivery to a rocky coast: Geology, v. 30, p. 895–898, doi:10.1130/0091-
230 7613(2002)030<0895:MMOWED>2.0.CO;2.
231 Agar, R., 1960, Post–glacial erosion of the North Yorkshire Coast from the Tees Estuary to
232 Ravenscar: Proceedings of the Yorkshire Geological Society, v. 32, p. 409–427,
233 doi:10.1144/pygs.32.4.409.
234 Allison, R.J., and Kimber, O.G., 1998, Modelling failure mechanisms to explain rock slope
235 change along the Isle and Purbeck coast, UK: Earth Surface Processes and Landforms, v. 23,
236 no. 8, p. 731–750, doi:10.1002/(SICI)1096-9837(199808)23:8<731::AID-
237 ESP885>3.0.CO;2-F.
238 Ashton, A., Walkden, M.J.A., and Dickson, M.E., 2011, Equilibrium responses of rocky coasts
239 to changes in the rate of sea level rise: Marine Geology, v. 284, p. 217–229,
240 doi:10.1016/j.margeo.2011.01.007.
241 Barlow, J., Lim, M., Rosser, N.J., Petley, D.N., Brain, M.J., Norman, E.C., and Geer, M., 2011,
242 Modeling cliff erosion using negative power law scaling of rockfalls: Geomorphology,
243 doi:10.1016/j.geomorph.2011.11.006.
244 Battjes, J. A., and Stive, M. J. F., 1985, Calibration and verification of a dissipation model for
245 random breaking waves, Journal of Geophysical Research-Oceans, 90(NC5), 9159- 9167.
246 Benumof, B.T., Storlazzi, C.D., Seymour, R.J., and Griggs, G.B., 2000, The relationship
247 between incident ave energy and seacliff erosion rates: San Diego County, California:
248 Journal of Coastal Research, v. 16, p. 1162–1178.

Collins, B.D., and Sitar, N., 2008, Processes of coastal bluff erosion in weakily lithified sands, Pacifica, California, USA: Geomorphology, v. 97, no. 3–4, p. 483–501, doi:10.1016/j.geomorph.2007.09.004.

Collins, B.D., and Sitar, N., 2011, Stability of steep slopes in cemented sands: Journal of Geotechnical and Geoenvironmental Engineering, v. 137, no. 1, p. 43–51, doi:10.1061/(ASCE)GT.1943-5606.0000396.

Dornbusch, U., Robinson, D.A., Moses, C.A., and Williams, R.B.G., 2008, Temporal and spatial variations of the chalk cliff retreat rate in East Sussex, 1873ents: Marine Geology, v. 249, p. 271–282, doi:10.1016/j.margeo.2007.12.005.

Emery, K.O., and Kuhn, G.G., 1982, Sea cliffs: Their processes, profiles and classification: Geological Society of America Bulletin, v. 93, p. 644–654, doi:10.1130/0016-7606(1982)93<644:SCTPPA>2.0.CO;2.

Furlani, S., Cucchi, F., and Odorico, R., 2010, A new method to study microtopographical changes in the intertidal zone: One year of TMEM measurements on a limestone removable rock slab (RRS): Zeitschrift fur Geomorphologie, v. 54, p. 137–151, doi:10.1127/0372-8854/2010/0054S2-0008.

Hampton, M.A., 2002, Gravitational failure of sea cliffs in weakly lithified sediment: Environmental & Engineering Geoscience, v. 8, no. 3, p. 175–191, doi:10.2113/8.3.175.

Hapke, C., and Green, K.R., 2006, Coastal landslide material loss rates associated with severe climatic events: Geology, v. 34, p. 1077–1080, doi:10.1130/G22900A.1.

Kogure, T., and Matsukura, Y., 2010, Critical notch depths for failure of coastal limestone cliffs: case study at Kuroshima Island, Okinawa, Japan: Earth Surface Processes and Landforms, v. 35, no. 9, p. 1044–1056.

Lim, M., Rosser, N.J., Allison, R.J., and Petley, D.N., 2010, Erosional processes in the hard rock coastal cliffs at Staithes, North Yorkshire: Geomorphology, v. 114, p. 12–21, doi:10.1016/j.geomorph.2009.02.011.

Limber, P.W., and Murray, B.A., 2011, Beach and sea-cliff dynamics as a driver of long-term rocky coastline evolution and stability: Geology, v. 39, p. 1147–1150, doi:10.1130/G32315.1.

Moses, C., and Robinson, D., 2011, Chalk cliff dynamics: Implications for understanding rock coast evolution: Earth-Science Reviews, v. 109, p. 3–4, 63–73, doi:10.1016/j.earscirev.2011.08.003.

Naylor L.A. and Stephenson, W.J. (2010). Spatial variations in weathering and erosion on shore platforms: a case of geological contingency? *Geomorphology*. 114:89-100. http://dx.doi.org/10.1016/j.geomorph.2008.12.024.

Naylor, L.A., Stephenson, W.J., and Trenhaile, A.S., 2010, Rock coast geomorphology: Recent advances and future research directions: Geomorphology, v. 114, no. 1–2, p. 3–11, doi:10.1016/j.geomorph.2009.02.004.

Nicholls, R.J., and Cazenave, A., 2010, Sea-level rise and its impact on coastal zones: Science, v. 328, p. 1517–1520, doi:10.1126/science.1185782.

Norman, E.C., 2012, Microseismic monitoring of the controls on rock cliff erosion [Unpublished Ph.D. thesis]: University of Durham, UK, http://etheses.dur.ac.uk/3586/.

Oppikofer, T., Jaboyedoff, M. & Keusen, H.-R. (2008): Collapse at the eastern Eiger flank in the Swiss Alps. Nature Geoscience, 1, 531 - 535. doi:10.1038/ngeo258.

Rawson, P.F., and Wright, J.K., 2000, The Yorkshire Coast: Geologists' Association Guide No. 34: Piccadilly, London, Burlington House,130 p.

Rosser, N., Lim, M., Petley, D.N., Dunning, S., and Allison, R.J., 2007, Patterns of precursory rockfall prior to slope failure: Journal of Geophysical Research, v. 112, F04014, doi:10.1029/2006JF000642.

Rosser, N.J., Petley, D.N., Lim, M., Dunning, S.A., and Allison, R.J., 2005, Terrestrial laser scanning for monitoring the process of hard rock coastal cliff erosion: Quarterly Journal of Engineering Geology and Hydrogeology, v. 38, p. 363–375, doi:10.1144/1470-9236/05-008.

Sanderson, F., Bakkehoi, S., Hestnes, E., and Lied, K., 1996, The influence of meteorological factors on the initiation of debris flows, rockfalls, rockslides, and rockmass stability, *in* Senneset, K., ed., Landslides: Rotterdam, Balkema. pp 97 – 114.

Schuerch, P., Densmore, A.L., Rosser, N.J., Lim, M., and McArdell, B.W., 2011, Detection of surfaces change in complex topography using terrestrial laser scanning: application to the Illgraben debris flow channel: Earth Surface Processes and Landforms, v. 36, p.1847-1859, doi:10.1002/esp.2206.

Senfaute, G., Duperret, A., and Lawrence, J.A., 2009, Micro-seismic precursory cracks prior to rock-fall on coastal chalk cliffs: A case study at Mesnil-Val, Normandie, NW France: Natural Hazards and Earth System Sciences, v. 9, p. 1625–1641, doi:10.5194/nhess-9-1625-2009.

Stock, G.M., Martel, S.J., Collins, B., and Harp, E.L., 2012, Progressive failure of sheetered rock slopes: The 2009–2010 Rhombus Wall rock falls in Yosemite Valley, California, USA: Earth Surface Processes and Landforms, v. 37, p. 546–561, doi:10.1002/esp.3192.

Styles, T.D., Coggan, J.S., and Pine, R.J., 2011, Back analysis of the Joss Bay chalk cliff failure using numerical modelling: Engineering Geology, v. 120, no. 1–4, p. 81–90, doi:10.1016/j.enggeo.2011.04.004.

Sunamura, T., 1982, A wave tank experiment on the erosional mechanism at a cliff base: Earth Surface Processes and Landforms, v. 7, p. 333–343, doi:10.1002/esp.3290070405.

Trenhaile, A.S., 2011, Predicting the response of hard and soft rock coasts to changes in sea level and wave height: Climatic Change, v. 109, p. 599–615, doi:10.1007/s10584-011-0035-7.

Viles, H., 2013, Linking weathering and rock slopes instability: Non-linear perspectives: Earth Surface Processes and Landforms, v. 38, p. 62–70, doi:10.1002/esp.3294.

Wolters, G., and Müller, G., 2008, Effect of cliff shape on the internal stresses and rock slope stability: Journal of Coastal Research, v. 24, no. 1, p. 43–50, doi:10.2112/05-0569.1.

Young, A.P., and Ashford, S.A., 2008, Instability investigation of Cantilevered Seacliffs: Earth Surface Processes and Landforms, v. 33, p. 1661–1677, doi:10.1002/esp.1636.

Young, A.P., Guza, R.T., O'Reilly, W.C., Flick, R.E., and Gutierrez, R., 2011, Short-term retreat statistics of a slowly eroding coastal cliff: Natural Hazards and Earth System Sciences, v. 11, p. 205–217, doi:10.5194/nhess-11-205-2011.

Figures

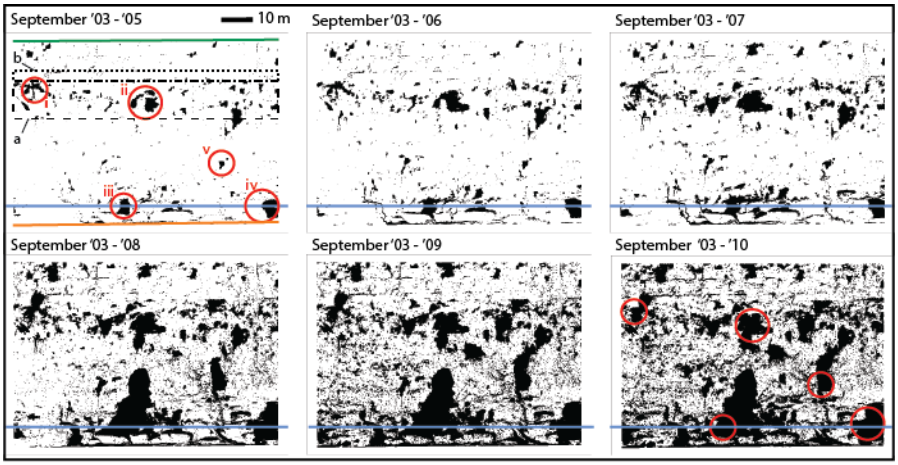

Dr N Rosser Figure 1 - 118 mm x 60 mm "Figure_1.eps"

Figure 1. Cumulative annual change at Site A between 3 September 2003 and 1 September 2010. Lines are: Green: cliff crest; Orange: cliff toe; Blue: Highest Astronomical Tide (HAT). Zones 'a' and 'b' are delimited by dashed and dotted lines. Red circles show: (i and ii) bridging and coalescence of sequential failures; (iii and iv) scars at the inundated cliff toe which propagate up-cliff; and (v) small scar which grows to coalesce forming a upslope aligned feature upon the cliff face.

Publisher: GSA
Journal: GEOL: Geology
Article ID: G34371

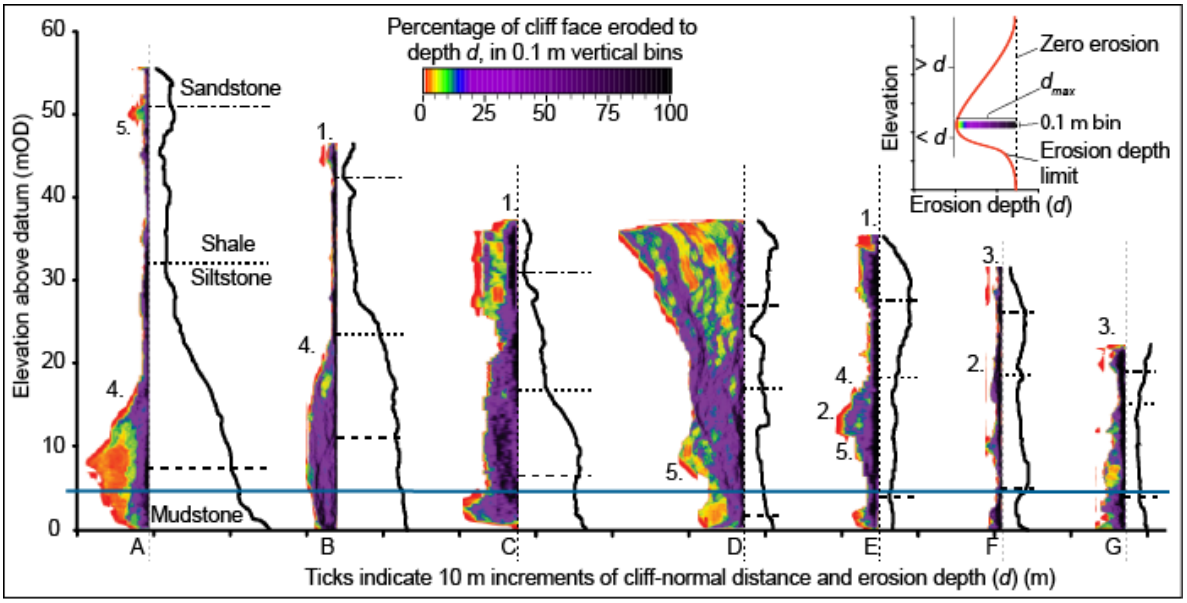

Figure 2. 7 years of cumulative erosion (3 September 2003–1 September 2010) monitored at sites A - G. Blue line shows highest astronomical tide (HAT) as the highest elevation experiencing inundation. Major geological contacts are delimited by dashed lines. Cliff slope profiles (solid black lines) were extracted from the 2010 laser scan. The vertical distribution of erosion depth (*d*) up cliff (colored shading) is shown at the same vertical and horizontal scale as the cliff profiles. For each 0.1 m elevation bin percentage of the cliff area eroding to depth *d* is calculated, where the vertical dotted line at each site represents zero erosion. Inset defines *d* and d_{max}, and general form of erosion pattern. Numerical labels indicate: (1) cliff line retreat; (2) isolated rockfall; (3) rockfall to discrete structurally defined depths; (4) gradual reduction of *d* with elevation; (5) rapid reduction of *d* below local maxima of *d*.

[1]GSA Data Repository item 2013xxx, xxxxxxxx, is available online at www.geosociety.org/pubs/ft2013.htm, or on request from editing@geosociety.org or Documents Secretary, GSA, P.O. Box 9140, Boulder, CO 80301, USA.

Publisher: GSA
Journal: GEOL: Geology
Article ID: G34371

GSA Data Repository

COASTLINE RETREAT VIA PROGRESSIVE FAILURE OF ROCKY COASTAL CLIFFS

Nick J. Rosser, Matthew J. Brain, David N. Petley, Michael Lim & Emma C. Norman

FIGURE DR1: Photograph of Site A taken from the foreshore during low tide, showing approximately the same spatial extent as the coverage of Figure 1. The site shown is approximately 55 m in height and 90 m in width.

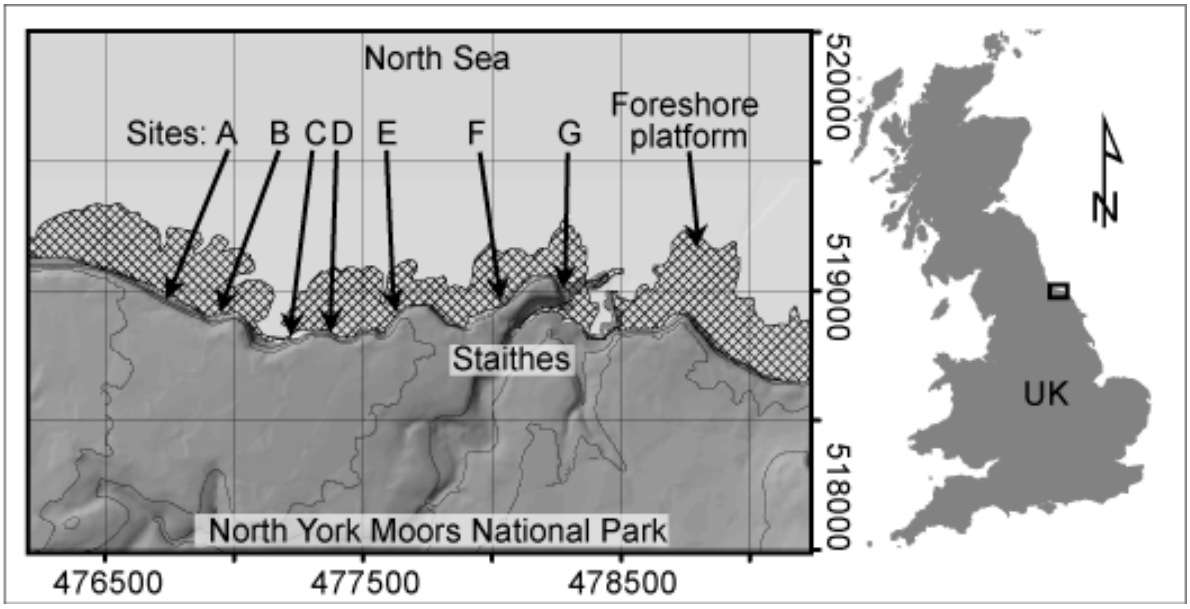

366

367 **FIGURE DR2:** Sites location on the coast of the North York Moors National Park (UK) coast.
368 Hatched area shows the foreshore platform. 25 m topographic contours to show the inland
369 topography, and are from Ordnance Survey PlanForm data (under license from EDINA, 2010).
370 Sites A – G were originally chosen to show a range of coastal planform settings (bays and
371 headlands), cliff heights (see: GSA Data Repository DRF), and covered an extent that could be
372 captured in surveys whilst access during a single tidal window was possible.
373

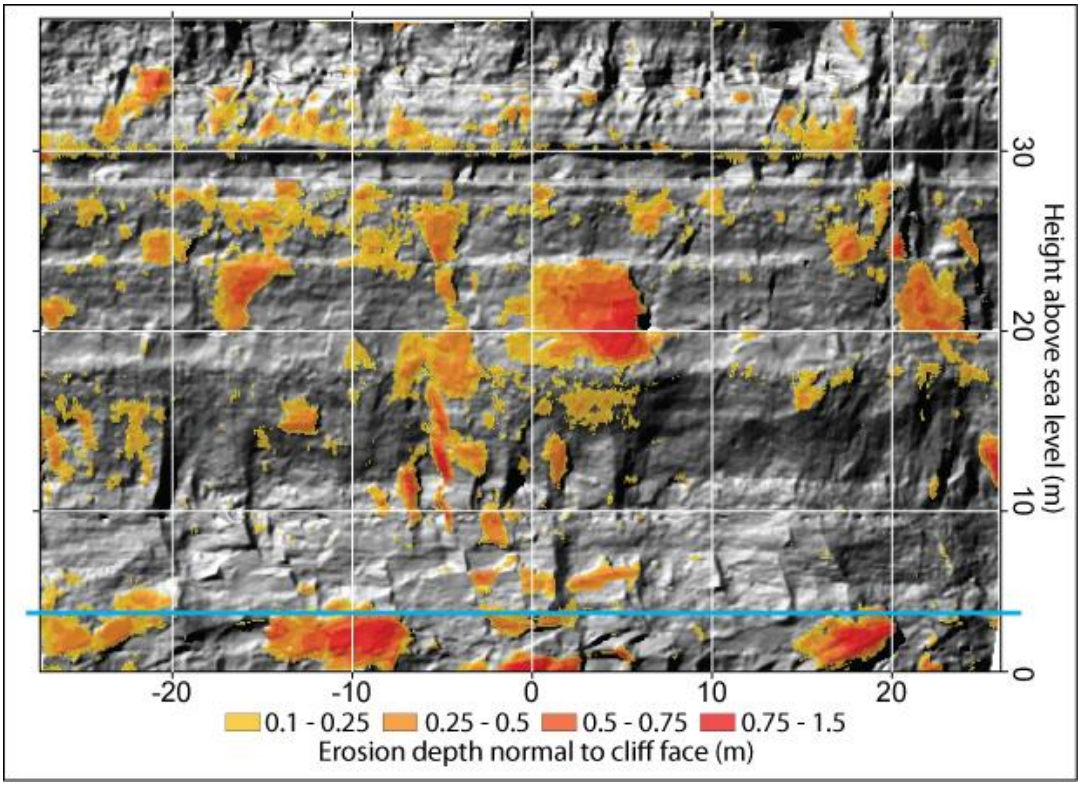

FIGURE DR3: Example of cliff erosion (Site F) derived from repeat terrestrial laser scanning between 01/09/03 and 03/09/10. The 2010 hillshade DEM of the cliff surface is superimposed with erosion depth (d), coloured by classified depth normal to the cliff face (m). T shows Highest Astronomical Tide (HAT).

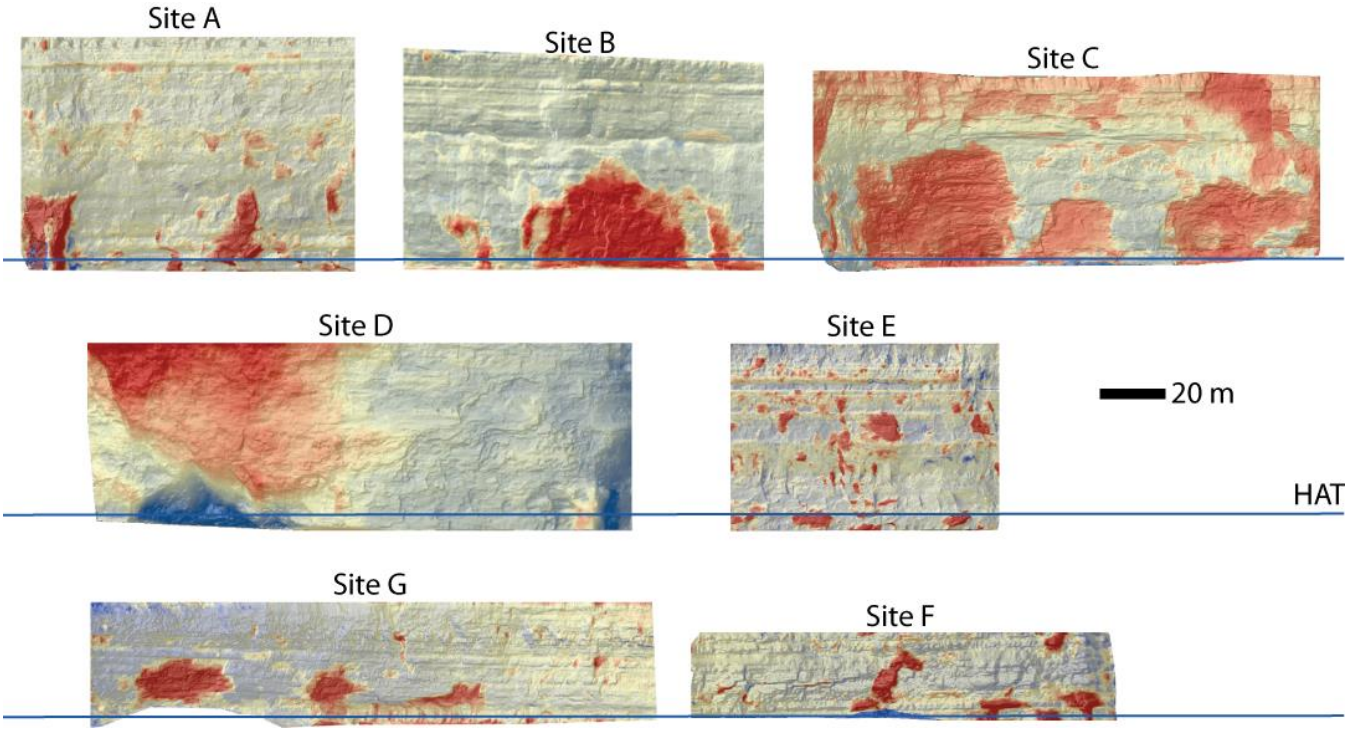

FIGURE DR4: Cliff face change as depth of rock lost normal to cliff strike, for Sites A – F between September '03 and September '10. Red colours show erosion; dark blue colours indicate accretion. Blue horizontal line shows inundation extent of Highest Astronomical Tide (HAT). Site D experience a full failure of the face, resulting in a c. 2,400 m^3 boulder deposit on the foreshore, some of which remained in September '10.

Publisher: GSA
Journal: GEOL: Geology
Article ID: G34371

389 **TABLE DR1: Monitored site geometry, erosion and retreat rates, 2003 – 2010**
390
391

Site	A	B	C	D	E	F	G	Mean
Cliff height (m)	55.33	47.00	37.81	37.78	36.50	32.25	21.85	38.36
Cliff width (m)	90.80	97.28	106.97	105.67	60.64	148.79	100.57	101.53
Projected area (m^2)	4,960.73	4,572.16	3,669.69	3,642.25	3,294.80	3,242.01	3,687.77	3,867.06
Active area (%)	15.86	38.34	45.79	44.13	16.05	25.13	22.30	29.66
Max erosion depth (m)	4.53	4.08	5.46	13.03	1.50	3.44	2.60	4.95
Erosion depth σ (m)	0.68	0.98	0.89	2.61	0.20	0.63	0.42	0.92
Total eroded volume (m^3)	145.69	1,673.59	229.46	2,023.76	165.31	540.09	278.00	722.27
Sediment yield ($kg^{-1} m^{-2} yr^{-1}$)	0.010	0.131	0.022	0.198	0.018	0.059	0.027	0.067
Standardised yield ($m^3 m^{-1} yr^{-1}$)	0.23	2.46	0.31	2.74	0.39	0.52	0.39	1.00
Dry cliff volume eroded (%)	78.28	84.74	83.38	76.90	79.01	93.26	86.63	83.17
Wet cliff volume eroded (%)	21.72	15.26	16.62	23.10	20.99	6.74	13.37	16.83
Annual retreat (m yr^{-1})	0.004	0.052	0.009	0.079	0.007	0.024	0.011	0.027
R_T (yr)	44.14	18.26	15.29	15.86	43.63	27.86	31.39	28.06
R_D (m)	0.19	0.95	0.14	1.26	0.31	0.66	0.34	0.55

Notes: Sediment yield calculation assumes rock density of c. 2.5 x 10^3 kg m^{-3}. Standardised yield is calculated per linear coastline m, per annum. R_T is the time in years for the whole cliff face to experience failure, assuming a random distribution of rockfalls. R_D is the depth of erosion which will be achieved during the period R_T. σ refers to the standard deviation of erosion depths (m).

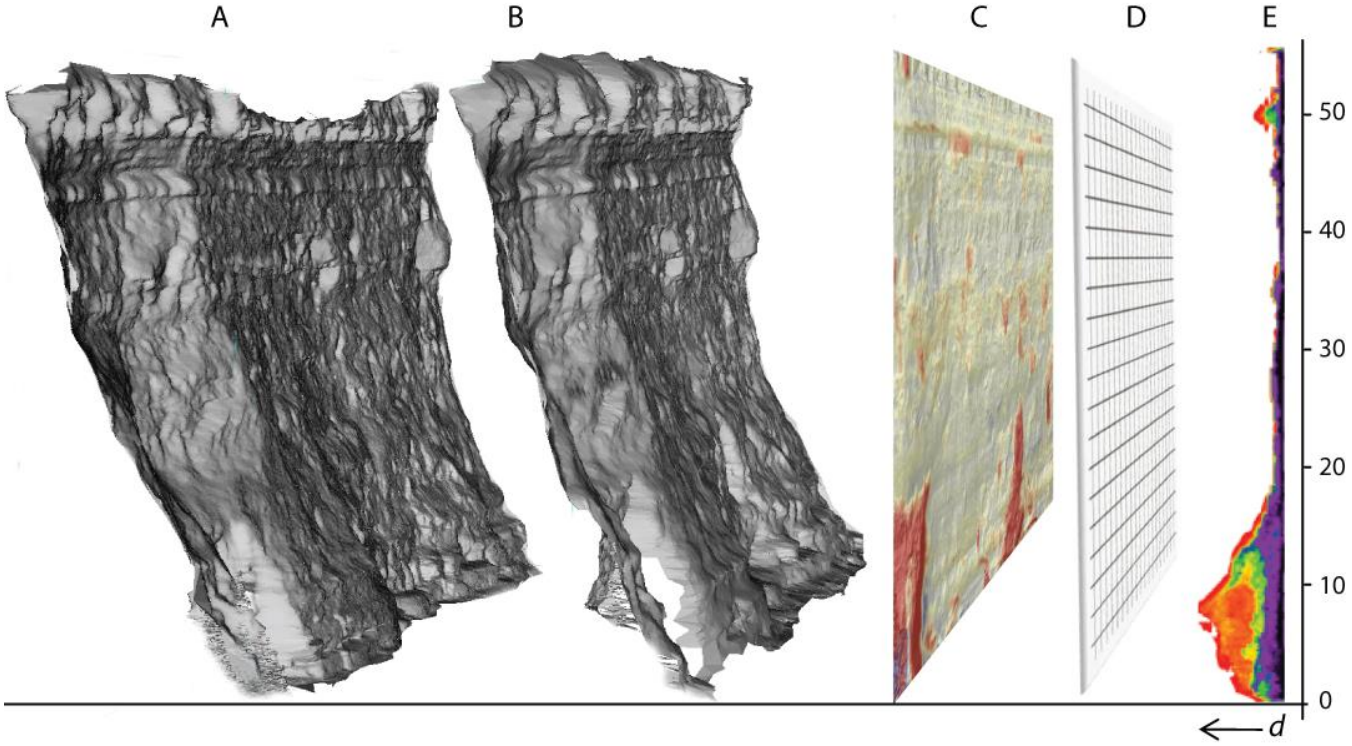

FIGURE DR5: Derivation of erosion profile data, showing data for Site A, 2003 – 2010. 3D laser scan point clouds are collected in month 1 and month n, and a surface generated for each using a 2.5D view dependant triangulation of the geo-referenced data, aligned relative to the view direction of the optical centre of the scanner (A and B). Change (*d*) is calculated for every vertex in A, by calculating the shortest distance to surface B. *d* is then gridded on a flat plane parallel to the dominant strike of the cliff face, at 0.1 m grid resolution (C). A grid (D), is used to sub-sample (C), from which the percentage of cells in each increment of elevation attain erosion depth *d*. This permits comparison between cliff sections of different profile form. Finally, erosion depth *d* is plotted against elevation, and colour-scaled relative to the percentage of the monitored cliff face within each 0.1 m elevation increment (E) experiencing erosion depth *d*.